IEEE Open Journal of
Power Electronics

Received 4 October 2021; revised 26 November 2021; accepted 5 December 2021. Date of publication 13 December 2021; date of current version 23 December 2021. The review of this paper was arranged by Associate Editor Lijun Hang.

Digital Object Identifier 10.1109/OJPEL.2021.3134714

A Per-Phase Power Controller for Smooth Transitions to Islanded Operation

TOMMASO CALDOGNETTO [1,2] (Senior Member, IEEE), HOSSEIN ABEDINI [1,2] (Student Member, IEEE), AND PAOLO MATTAVELLI [1,2] (Fellow, IEEE)

[1]Department of Management and Engineering, University of Padova, Vicenza 36100, Italy
[2]Interdepartmental Centre Giorgio Levi Cases, University of Padova, Padova 35131, Italy

CORRESPONDING AUTHOR: TOMMASO CALDOGNETTO (e-mail: tommaso.caldognetto@unipd.it)

This work was supported in part by the Interdepartmental Centre Giorgio Levi Cases, under Project "NEBULE," and in part by the Department of Management and Engineering, under Project "ADPE," University of Padova.

ABSTRACT This paper presents a droop-based controller for grid-tied three-phase inverters. The controller allows to regulate the inverter output power while operating grid-tied, to support the local grid voltage while operating islanded, and to seamlessly transition into this latter mode of operation. Remarkably, the use of the traditional droop control scheme for per-phase power control would lead to unequal frequencies among the phase voltages, which is not acceptable. Instead, the proposed controller allows independent power references tracking at each of the phases of a three-phase inverter while grid-tied and a proper transition into the islanded operation. Per-phase power control is crucial for several services in modern smart power networks, like demand-response and distributed unbalance compensation. The paper also reports the stability analysis of the whole control system and outlines a procedure for the design of the involved regulators. Simulation and experimental results considering a laboratory-scale prototype are reported and discussed to validate the proposed controller.

INDEX TERMS Converter control, droop-control, grid-tied inverters, microgrids, power control, unbalanced power control.

I. INTRODUCTION

Low-voltage grids are steadily evolving to provide the advanced services that are required in the forthcoming energy scenario [1], [2]. Examples of crucial features are *i*) flexible power control, to allow resilience to variable power demand [3] and participation to transactive energy markets [4], *ii*) continuity of service, via islanded operation in response to adverse localized events interrupting the mainstream electricity supply, and *iii*) optimal power quality, in terms of power factor and balanced power absorption [5].

The variegate requirements are commonly managed via hierarchical control systems, as shown in Fig. 1, of which the droop control constitutes the primary layer [2], [6]. Droop control with electronic power converters (EPCs) controlled as voltage sources is indeed widely used in ac microgrids [7], [8]. It sports the advantage of supporting the grid voltage and the capability of adapting the inverters voltage references so as to automatically share the power needs in islanded grids [8]. Actually, droop controlled EPCs are often referred to as playing a grid-forming functionality, in the sense that the grid voltage is determined by their aggregate contribution [9]. Fig. 1 also reports the, so called, zero-level control, consisting of voltage and current controllers receiving reference signals from the primary controller [2], [6], [10]. Various choices are possible for zero-level control implementation [10]–[13], herein, natural reference frame *abc* with linear voltage and current regulators is considered.

On the other hand, output power control requires specific provisions. Two opposite needs are present, namely, *i*) supporting the grid voltage by adapting the inverter output power according to the droop laws, useful especially during islanded operation [14], *ii*) making the output power fixed and independent from grid voltages and loading conditions to allow power control, useful especially during grid-tied operation [12], [13].

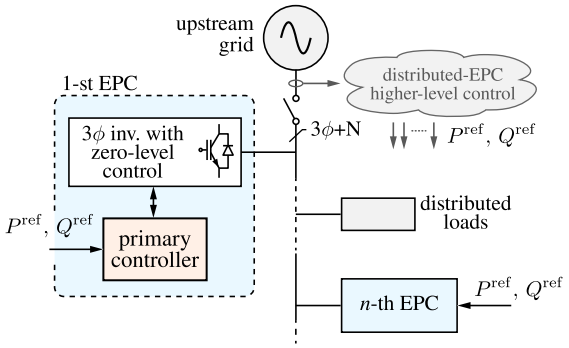

FIGURE 1. Microgrid scenario with islanded capabilities and distributed electronic power converters (EPCs) accepting power references issued by higher-level control methods. The proposed solution relates to the primary controller block.

These are requirements also considered in latest relevant standards, like, for example, [15]. In [16] the two needs are accomplished considering the *total* power delivered by the inverter, but *per-phase* power control is not possible by the control scheme in [16] without loosing the property of smooth transitions into islanded operation.

However, independent power control of each phase is necessary in several circumstances. In smart electricity grids, distributed EPCs can receive power references computed by optimization algorithms that pursue control goals like loss and current stress minimization. The related application scenarios extend those of uninterruptible power supply systems (UPS) [17], [18], in which the main focus is on providing uninterrupted supply to the served loads, while in Fig. 1 power control is an important feature too. For example, [19] proposes a centralized controller that issues optimal per-phase power references to distributed three-phase EPCs, achieving power-flow controllability at the point of common coupling (PCC) of a microgrid with the upstream grid. Independent power control is shown in [20] to solve serious power quality issues due to unbalance and nonlinear loads in distribution networks, in which EPCs capable of flexibly regulating their injected per-phase power would induce greater loss reduction and remarkable power-quality improvements [21]. Similar results are reported in [5], [22]–[24]. Per-phase power control is useful in isolated master-slave microgrid architectures too, where centralized controllers with one or multiple master EPCs are present to improve microgrid operation [14], [25]. In such microgrids, per-phase control allows to support the master units in generating the power requests from the loads at the different phases, as shown in [26]. In general, flexible power control is crucial to achieve the control goals aimed for in the, continuously evolving, smart power systems scenario [15], [27].

Solutions have been presented in the literature for the per-phase control of active-power sharing on four-wire microgrids under unbalanced loads [28], [29], but output power tracking is not considered. On the other hand, the literature reports per-phase output power controllers, like [30], but without considering or including islanded operation capabilities. In fact, the use of the traditional droop control scheme for per-phase power control would lead to unequal frequencies among the phase voltages at the transition to the islanded operation, that is, an unacceptable desynchronization among the phases. To the authors' knowledge, there is a lack of solutions considering per-phase power flow control while preserving the feature of seamlessly transition from the grid-connected into the islanded operation modes.

This paper proposes a controller for grid-tied three-phase EPCs, displayed in Fig. 2, addressing the challenges discussed above. Specifically, the proposed solution features *i*) independent output power control for each phase of a three-phase four-wires grid-connected inverter, *ii*) smooth transitions into the islanded operation mode, *iii*) operation in islanded conditions, even when multiple parallel connected EPCs integrating the proposed controller are present. The controller is also modeled analytically and analyzed, finally discussing a simple design procedure.

This paper extends [31], presenting additional details on the control principle, analyses, and experimental results. In the following, the control scheme is presented in Section II, its analysis and design is discussed in Section III. Section IV reports simulation and experimental results showing the obtained controller behavior. Section V concludes the paper.

II. PER-PHASE CONTROL PRINCIPLE

The control principle is to synchronize the inverter by considering the total three-phase active power delivered by the inverter itself and, while operating grid-connected, to achieve per-phase output active and reactive power regulation by adjusting the phase-shift and the voltage amplitude, respectively, of each phase independently. By extending the approach in [16], saturated controllers are employed to perform power control and achieve smooth transitions into the islanded operation.

Fig. 3 shows the block diagram of the proposed controller, where the generic x-th phase, $x \in \{a, b, c\}$, is represented. At the top of the figure, a P-f droop relation processes the total three-phase power $P_{3\phi}$ exchanged at the inverter output and provides the angle $\varphi_{3\phi}$, which is the integral of the angular frequency given by the traditional droop characteristic:

$$\omega^* = \omega_0 + k_{p,3\phi}\left(P^*_{3\phi} - P_{3\phi}\right) \tag{1}$$

where ω_0 is the nominal frequency, $k_{p,3\phi}$ is the droop coefficient, and $P^*_{3\phi}$ is a reference three-phase power [8]. The phase angle $\varphi_{3\phi}$, rotating at frequency ω^*, is synchronized with the grid and used to derive the angle of each of the phases, as illustrated in Fig. 4. In this way, the synchronization capability of the droop control [32] is retained and exploited. The top branch in Fig. 3 is called synchronization branch hereinafter.

The angle φ_x of each phase is computed by adding to the synchronized angle $\varphi_{3\phi}$ the nominal phase angle φ_x^{nom} of the specific phase (i.e., 0, $-2/3\pi$ or $+2/3\pi$ for phases a, b, c, respectively) and by adjusting the result by the quantity $\Delta\varphi_x$

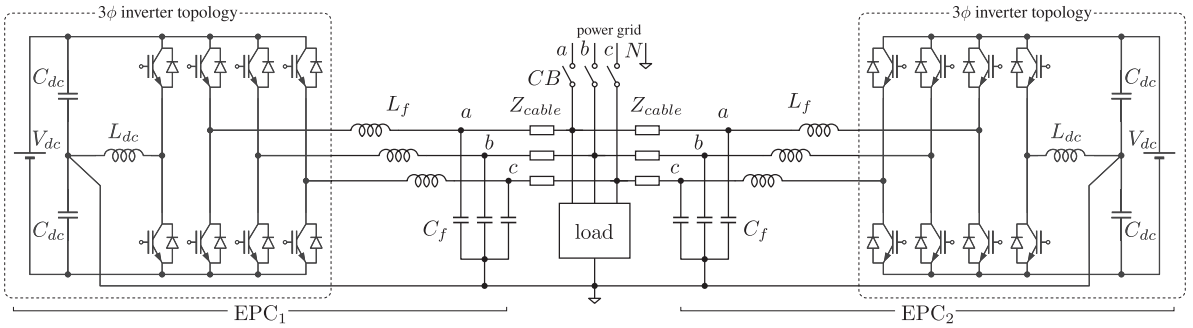

FIGURE 2. Electronic power converters (EPCs) connected to a three-phase four-wire low-voltage network.

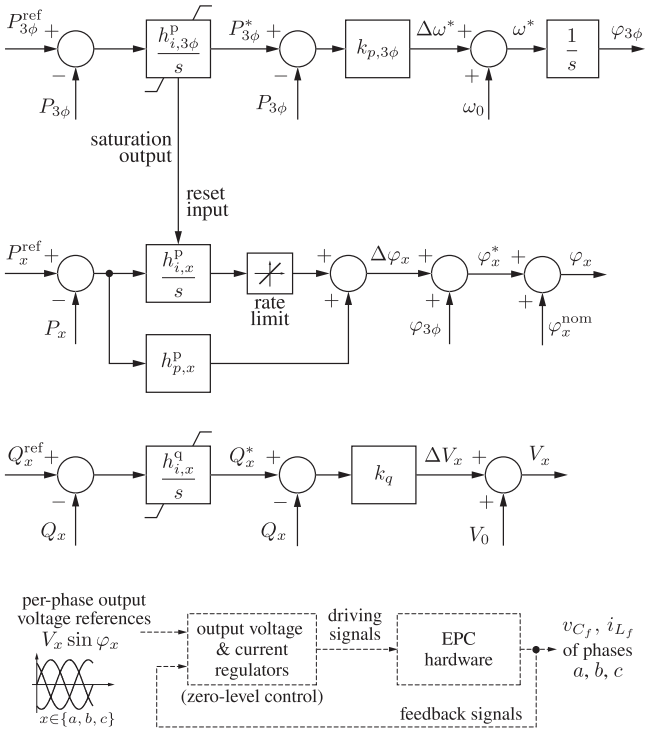

FIGURE 3. Per-phase power controller. The top, synchronization branch provides a reference angle $\varphi_{3\phi}$ to the three phases, represented by the generic symbol x (i.e., a, b, c). The angle and amplitude of each phase are adjusted for per-phase power control. The resulting references $V_x \sin \varphi_x$ are given to EPC current and voltage regulators (zero-level control) for output voltage control.

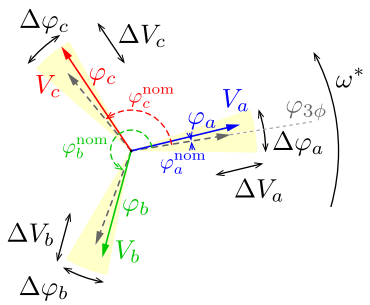

FIGURE 4. Controlled quantities by the proposed per-phase control. Highlighted the possible phase variations $\Delta\varphi_x$ and amplitude variations ΔV_x for the desired active and reactive, respectively, per-phase power exchange.

that aims at the desired active power P_x at phase x. Nominal voltage amplitudes V_0 are similarly adjusted by the quantity ΔV_x for reactive power control. The instantaneous voltage reference value for the x-th phase results:

$$V_x \sin(\varphi_x) = (V_0 + \Delta V_x) \sin\left(\varphi_{3\phi} + \Delta\varphi_x + \varphi_x^{\text{nom}}\right) \tag{2}$$

where $\varphi_{3\phi}$ is the integral of the frequency ω^*, as indicated while introducing (1), while ΔV_x and $\Delta\varphi_x$ are constant terms in steady-state. Notably, variations $\Delta\varphi_x$ and ΔV_x are relatively small and depend on the injected power and the interconnection impedances among sources. As commonly done with droop control, mainly inductive interconnection impedances are considered herein, which may be related to the characteristics of the grid or it may be imposed by proper converter control provisions [6], [8].

The controllers computing the introduced quantities, displayed in Fig. 4, are discussed in the following.

A. GRID-CONNECTED OPERATION

In order to achieve total three-phase output power tracking, which is possible during grid-tied operation [33], $P_{3\phi}^*$ is adjusted by a three-phase power regulator:

$$H_{3\phi}^{\text{p}}(s) = \frac{h_{i,3\phi}^{\text{p}}}{s} \tag{3}$$

Its control action modifies the total three-phase power $P_{3\phi}$ delivered by the inverter.

To achieve per-phase power tracking, the obtained $\varphi_{3\phi}$ is then adjusted phase-by-phase as displayed by the central blocks in Fig. 3, referring to the generic x-th phase. Here, a proportional-integral controller, denoted as:

$$H_x^{\text{p}}(s) = h_{p,x}^{\text{p}} + \frac{h_{i,x}^{\text{p}}}{s} \tag{4}$$

produces the phase shift $\Delta\varphi_x$ that adds to the instantaneous three-phase angle $\varphi_{3\phi}$ and allows the phase power P_x to follow the respective reference power P_x^{ref} during grid-tied operation.

B. ISLANDED OPERATION

Within an islanded subsystem, the generated and dissipated power must balance exactly, therefore, a transition into islanded operation makes output power control no more possible and automatically leads the power regulator $H_{3\phi}^{\text{p}}$ in (3)

into saturation. Consistently, the integral part of the per-phase regulator H_x^{p} defined in (4) is also disabled, as shown in Fig. 3. The saturation limits $P_{3\phi}^{*\max}$ or $P_{3\phi}^{*\min}$ can be designed considering the principles presented in [16], and reviewed in the next Section III-B. Remarkably, during the islanded mode of operation, the controller behaves as a traditional droop controller, by which the converter frequency ω^* changes linearly with the total delivered three-phase power:

$$\omega^* = \omega_0 + k_{p,3\phi}\left(P_{3\phi}^{*\mathrm{sat}} - P_{3\phi}\right) \tag{5}$$

where $P_{3\phi}^{*\mathrm{sat}}$ is a constant saturation limit, namely, $P_{3\phi}^{*\max}$ or $P_{3\phi}^{*\min}$, further discussed in the following Section III-B.

For what concerns reactive power control, per-phase reactive power control is more straightforward, because it acts on the amplitude of the generated voltages and does not affect the phases of the voltages, which are critical for synchronization. Then, a simple saturated controller can be directly applied to each phase, as described in [16].

Finally, it is worth to highlight the use of a rate limiter at the output of the integral part of H_x^{p}, which gradually brings to zero the corresponding phase adjustment when it is not required (i.e., during islanded operation). Instead, the proportional part can be optionally kept, in order to improve the dynamics and power sharing among multiple inverters operating in parallel [14], [28], [34], [35].

III. STABILITY ANALYSIS AND CONTROL DESIGN

The controller described in Section II presents two operation modes, namely, the grid-connected and the islanded operation modes. In the former operation mode, the controller $H_{3\phi}^{\mathrm{p}}$ in the synchronization branch and the per-phase power controllers H_x^{p} are active. Differently, during islanded operation, these regulators saturate, which reduces the control system dynamics to those of the traditional droop control, where the converter frequency ω^* changes linearly with the total delivered three-phase power, as in (5). This latter operation mode is analyzed in many relevant papers [36], [37], while the grid-connected behavior is peculiar to the proposed solution and it is analyzed next.

A. SMALL-SIGNAL ANALYSIS

Let us model the EPC by its Thevenin's representation, as a voltage source with series output impedance, operating connected to a voltage source representing the grid voltage [36]. Be $V_x\angle\varphi_x$ the EPC voltage, $V_g\angle 0$ the grid voltage, ω_g the system frequency and $Z\angle\theta_Z$ the EPC output impedance. The active and reactive power exchange among the two sources considering the generic x-th phase result [36], [38]:

$$P_x = \frac{V_g}{Z}\left[\left(V_x\cos\varphi_x - V_g\right)\cos\theta_Z + V_x\sin\theta_Z\sin\varphi_x\right] \tag{6}$$

$$Q_x = \frac{V_g}{Z}\left[\left(V_x\cos\varphi_x - V_g\right)\sin\theta_Z - V_x\cos\theta_Z\sin\varphi_x\right] \tag{7}$$

Assuming a mainly inductive impedance $Z = j\omega_g L_x$ and small phase-differences between the inverter output voltage and the grid voltage, the following simplified model can be derived:

$$P_x \simeq \frac{V_g V_x}{\omega_g L_x}\varphi_x \tag{8}$$

$$Q_x \simeq \frac{V_g\left(V_x - V_g\right)}{\omega_g L_x} \tag{9}$$

Based on (8) and (9), the small-signal model of the control system in Fig. 3 and the plant can be derived for stability analysis and regulators design.

The system phase at the output of the synchronization branch, top of Fig. 3, is:

$$\varphi_{3\phi} = \frac{1}{s}\left[\omega_0 + k_{p,3\phi}\left[H_{3\phi}^{\mathrm{p}}\sum_x\left(P_x^{\mathrm{ref}} - P_x\right) - \sum_x P_x\right]\right] \tag{10}$$

where $H_{3\phi}^{\mathrm{p}}$ is defined in (3). The three per-phase output powers can be written by using (8) as:

$$P_x = \frac{V_x V_g}{\omega_g L_x}\left[H_x^{\mathrm{p}}\left(P_x^{\mathrm{ref}} - P_x\right) + \varphi_{3\phi} + \varphi_x^{\mathrm{nom}}\right] \tag{11}$$

where, to simplify the notation, the equal sign is used in the sense of small-signal linearized modelling. By collecting the per-phase quantities in column vectors, which are denoted hereafter by a bar [e.g., $\bar{P} = (P_a, \ldots, P_c)^T$ for the per-phase powers P_x, $x = a, b, c$], (10) and (11) can be written in matrix form for the three-phase system as:

$$\varphi_{3\phi} = \frac{1}{s}\left[\bar{\omega}_0 + k_{p,3\phi}\left[H_{3\phi}^{\mathrm{p}}\mathbb{1}_3^T\left(\bar{P}^{\mathrm{ref}} - \bar{P}\right) - \mathbb{1}_3^T\bar{P}\right]\right] \tag{12}$$

$$\bar{P} = \Gamma\left[H_x^{\mathrm{p}}\left(\bar{P}^{\mathrm{ref}} - \bar{P}\right) + \varphi_{3\phi}\mathbb{1}_3 + \bar{\varphi}^{\mathrm{nom}} - \bar{\varphi}_G\right] \tag{13}$$

where $\mathbb{1}_3$ is a 3×1 column vector of ones, Γ is a 3×3 diagonal matrix with elements $V_x V_g/\omega_g L_x$, and $\bar{\varphi}_G$ represents the instantaneous phase of the grid voltages.

For stability analysis, the exogenous inputs appearing in (12) and (13), namely, $\bar{\omega}_0$, $\bar{P}^{\mathrm{ref}}$, $\bar{\varphi}^{\mathrm{nom}}$, and $\bar{\varphi}_G$, can be neglected, yielding:

$$\varphi_{3\phi} = \frac{1}{s}k_{p,3\phi}\left(-H_{3\phi}^{\mathrm{p}}\mathbb{1}_3^T - \mathbb{1}_3^T\right)\cdot\bar{P} \tag{14}$$

$$\bar{P} = \left(I_3 + H_x^{\mathrm{p}}\Gamma\right)^{-1}\Gamma\cdot\left(\varphi_{3\phi}\mathbb{1}_3\right) \tag{15}$$

where I_3 represents the 3×3 identity matrix. Finally, (14) and (15) allow to write the loop gain of the control loop involving $\varphi_{3\phi}$:

$$T_{\varphi_{3\phi}} = \frac{1}{s}k_{p,3\phi}\left(H_{3\phi}^{\mathrm{p}} + 1\right)\mathbb{1}_3^T\left(I_3 + H_x^{\mathrm{p}}\Gamma\right)^{-1}\Gamma\,\mathbb{1}_3 \tag{16}$$

and to analyze the poles of the closed-loop system, which correspond to the zeroes of $1 + T_{\varphi_{3\phi}}$. This is performed in the experimental Section IV, considering the used prototype parameters.

B. CONTROLLER DESIGN

The design of the controller $H^{\mathrm{p}}_{3\phi}$ in the synchronization branch and of the per-phase controllers H^{p}_{x} can be performed on the basis of the analysis presented above.

Time-scale separation is exploited in the following, for a practical design procedure of the two regulators. Specifically, the loop involving $H^{\mathrm{p}}_{3\phi}$ is designed faster than the per-phase power control loops involving H^{p}_{x}, which allows to neglect the effect of the per-phase controller (i.e., terms φ_x are assumed constant) while considering the design of $H^{\mathrm{p}}_{3\phi}$. Under this assumption, and by noticing that the resulting regulation loop is in a unitary feedback configuration, the loop gain relevant to $H^{\mathrm{p}}_{3\phi}$ can be written as:

$$T_{P_{3\phi}} = \frac{k_{p3\phi}\frac{1}{s}\left(3\frac{V_x V_g}{\omega_g L_x}\right)}{1 + k_{p3\phi}\frac{1}{s}\left(3\frac{V_x V_g}{\omega_g L_x}\right)} = \frac{1}{1 + s/\omega_{p,3\phi}},$$

$$\omega_{p,3\phi} = k_{p3\phi}\left(3\frac{V_x V_g}{\omega_g L_x}\right) \tag{17}$$

Similarly, the loop-gain relevant to the per-phase controller H^{p}_{x} is:

$$T_{P_x} = \frac{V_g V_x}{\omega_g L_x} \tag{18}$$

which is a constant term. On this basis, the regulators coefficients $h^{\mathrm{p}}_{i,3\phi}$ with (17) and $h^{\mathrm{p}}_{p,x}$ and $h^{\mathrm{p}}_{i,x}$ with (18) can be easily found.

On the light of the considerations above, parameter settings of the controller in Fig. 3 may be performed as follows.

1) The droop coefficients are set, as commonly done, considering the maximum frequency and voltage variations, namely, $\Delta\omega_g^{\max}$ and $\Delta V^{\max}$, respectively, and the converter rated power S_N:

$$k_{p,3\phi} = \frac{\Delta\omega_g^{\max}}{2S_N} \qquad k_q = \frac{\Delta V_g^{\max}}{2S_N} \tag{19}$$

2) The three-phase regulator integrative gain is set considering the loop-gain (17). For example, by basic regulators design, if a phase-margin of at least 60 deg is targeted, the chosen crossover frequency $\omega_{cross,3\phi}$ should not exceed about a half of the pole frequency $\omega_{p,3\phi}$ in (17). Under this assumption, the integrative gain can be set to:

$$h^{\mathrm{p}}_{i,3\phi} = \omega_{cross,3\phi} \tag{20}$$

3) The per-phase reactive power regulator can be set as done in [16], being it possibile to set the voltage amplitude of each phase independently from the voltage amplitude of the other phases.
4) The per-phase power regulator H^{p}_{x} can be set considering the loop gain (18) and a crossover frequency significantly smaller than the one set for the synchronization control loop $\omega_{cross,3\phi}$.

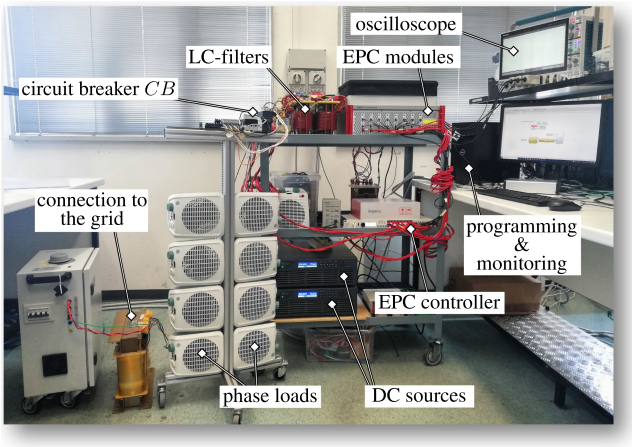

FIGURE 5. Photo of the experimental setup implementing the system in Fig. 2.

TABLE 1 Inverters (EPCs) Parameters

Parameter		Value
dc-link voltage	V_{dc}	350 V
dc-link capacitor	C_{dc}	3.3 mF
dc-link inductor	L_{dc}	2.5 mH
output filter capacitor	C_f	50 μF
output filter inductor	L_f	1.5 mH
switching frequency	f_{sw}	20 kHz
nominal power rating	S_N	3 kVA
nominal grid voltage rms	V_g^{nom}	110 V
nominal grid frequency	ω_g^{nom}	$2\pi \cdot 50$ rad/s
grid frequency range	$\omega_g^{\min}, \omega_g^{\max}$	$2\pi \cdot [49, 51]$ rad/s

5) The saturation limits are set to ensure power reference tracking within the whole allowed frequency and voltage range, as described in [16], that is:

$$P^{*\max}_{3\phi} = -P^{*\min}_{3\phi} = S_N + \frac{\Delta\omega_g^{\max}}{2k_{p,3\phi}} \tag{21}$$

$$Q^{*\max}_{x} = -Q^{*\min}_{x} = \frac{S_N}{3} + \frac{\Delta V_g^{\max}}{2k_q} \tag{22}$$

notably, these limits are fixed and depend on the nominal parameters of the EPC and the grid.

IV. EXPERIMENTAL RESULTS

The proposed controller was tested in simulation and by means of a laboratory-scale experimental prototype visible in Fig. 5 implementing the system in Fig. 2. The main hardware parameters are reported in Table 1. The converters were implemented using eight Imperix PEB8032 half-bridge modules, while the controller was deployed on an Imperix B-Box RCP embedding a Xilinx Zynq 7030 SoC. All the control blocks were executed once per switching period on the DSP module of the Xilinx SoC while the modulators and the protection blocks were executed on its FPGA module. As visible in Fig. 2, a split-link inverter with active balancing is used in the prototype to control the neutral-point voltage despite of

TABLE 2 Control Parameters

Parameter		Value	
P-f droop coefficient	$k_{p,3\phi}$	0.28571	mHz/W
V-Q droop coefficient	k_q	1.6	mV/VAr
3-phase P contr. integ. gain	$h^{\mathrm{p}}_{i,3\phi}$	8	1/s
3-phase P saturation limit (21)	$P^{*\,\max}_{3\phi}$	± 7	kW
per-phase P contr. integ. gain	$h^{\mathrm{p}}_{i,x}$	0.875	mrad/Ws
per-phase P contr. prop. gain	$h^{\mathrm{p}}_{p,x}$	49.867	μrad/W
per-phase Q contr. integ. gain	$k^{\mathrm{q}}_{i,x}$	180	1/s
per-phase Q saturation limit (22)	$Q^{*\,\max}_{x}$	$\pm 7/3$	kVAr
nominal voltage amplitude	V_0	$\sqrt{2}\cdot 110$	V
nominal frequency	ω_0	$2\pi\cdot 50$	rad/s
maximum frequency variation	$\Delta\omega_g^{\max}$	4	% ω_0
maximum voltage variation	$\Delta V_g^{\max}$	10	% V_0

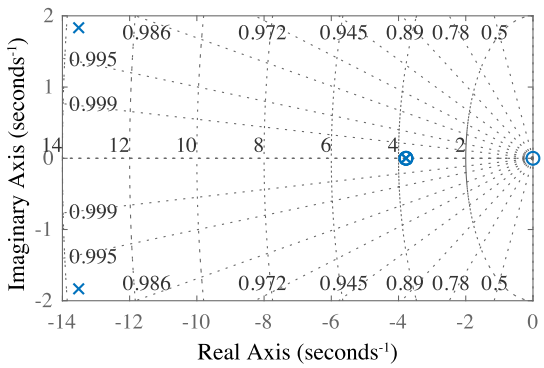

FIGURE 6. Pole-zero plot of the controller in Fig. 3 coupled with the system in Fig. 2 and with parameters in Table 1 and Table 2.

the presence of neutral currents while supplying unbalanced powers, as done in [39]. Other solutions may be successfully adopted too [40], [41]. Besides, any other inverter topologies with related zero-level control, namely, current and voltage regulators, capable of imposing the line to neutral voltages, including, for example, multi-level converters and other more advanced topologies, may be used for the implementation of the circuit enclosed in the dashed box in Fig. 2.

The controller is designed by the procedure described in Section III-B, resulting in the parameters listed in Table 2. The dynamics of the obtained closed-loop control can be studied by the analysis in Section III-A, specifically, the loop-gain $T_{\varphi 3\phi}$ in (16). Fig. 6 displays the pole-zero plot of the transfer function $1/(1+T_{\varphi 3\phi})$. Notably, the system presents stable and well damped poles, all lying on the right-half-plane.

The measured performance of the controller considering the described experimental setup are reported in the following. Six conditions are considered, specifically, unbalance power reference step variation, balance power reference step variation, grid-tied to islanded transitions, parallel operation while islanded, reactive power control, and islanded to grid-connected transition.

Comparisons with simulation results are also reported. The models were developed in Matlab/Simulink to implement the controller, in Fig. 3, coupled with the Thevenin's representation of the EPC and the grid, consistently with the assumptions made at the beginning of Section III-A. The equivalent output inductance of EPCs was set to 3.5 mH by zero-level control.

Fig. 7 and Fig. 8 display the most significant experimental waveforms. Besides the instantaneous three-phase voltages that are always reported, the subfigures on the left display the measured output current for each phase and the phase displacement with respect to the first phase (i.e., $\varphi_b^* - \varphi_a^*$ and $\varphi_c^* - \varphi_a^*$), the subfigures on the right display the voltage amplitudes ΔV_a, ΔV_b, and ΔV_c and the frequency deviation $\Delta\omega^*$. The results are discussed in the following.

A. UNBALANCED POWER REFERENCE STEP VARIATION

Fig. 7(a)-(b) displays the response to a step change of the output power reference of a phase during grid-connected operation with EPC_1 connected to the main grid while EPC_2 is disabled. In this test, a reference step $P_c^{\mathrm{ref}} : 0 \rightarrow 1\,\mathrm{kW}$ is applied, while all the other active and reactive power references are kept to zero. Fig. 7(a) shows that only phase-c increases the delivered current while the currents of the other phases—that are displayed with magnified scale—show just small, transient variations. A major phase displacement is observed in phase-c due to the increased power injection. Fig. 7(b) displays the evolution of references V_1, V_2, and V_3, by means of the voltage variations ΔV_x, and the frequency variation $\Delta\omega^*$. Variations can be observed on phase-c due to not perfectly inductive interconnection impedances (measured X/R ratio of about 4.5), while ω^* does not change in steady-state, being it fixed by the main grid voltage.

Using the acquired waveforms, it is possible to compute the delivered per-phase active power and compare the results with the simulation models used to validate the analysis presented in Section III-A. This is done in Fig. 9(a), which shows good correspondence among simulation and experimental results.

B. BALANCED POWER REFERENCE STEP VARIATION

Fig. 7(c)-(d) displays the response to a step change of the power reference of all the three-phases during grid-connected operation with EPC_1 connected to the main grid while EPC_2 is disabled. In this test, a reference step $P_x^{\mathrm{ref}} : 0 \rightarrow 1\,\mathrm{kW}$ is applied, while reactive power references are kept to zero. Fig. 7(c)-(d) show that the whole three-phase voltage frame angle $\varphi_{3\phi}$ is mainly adjusted under the effect of $\Delta\omega^*$ in the upper block in Fig. 3, bringing to negligible variations of phase displacements $\varphi_b^* - \varphi_a^*$ and $\varphi_c^* - \varphi_a^*$. This results from the time-scale separation adopted in Section III-B. Fig. 7(d) displays analogous variations in voltage amplitude. Frequency ω^* is unchanged in steady-state due to the presence of the main grid.

As done considering the previous unbalanced test, for the aim of validation, Fig. 9(b) displays the obtained results from the simulation and the experimental test. A good correspondence among simulation and experimental results can be remarked.

FIGURE 7. Experimental results with EPC_1 in Fig. 5 implementing the proposed control scheme in Fig. 3. (a)-(b) reference step change $P_c^{ref}: 0 \rightarrow 1$ kW with balanced load of 13 Ω; (c)-(d) reference step change of all the phases $P_{a,b,c}^{ref}: 0 \rightarrow 1$ kW with balanced load of 13 Ω; (e)-(f) transition into the islanded operation with balanced load of 25 Ω; (g)-(h) transition into the islanded operation of EPC_1 and EPC_2 with balanced load of 12.5 Ω and grid frequency of 50.22 Hz.

C. GRID-TIED TO ISLANDED TRANSITION

Fig. 7(e)-(f) displays the response to a transition from the grid-connected to the islanded operation modes with EPC_1 initially connected to a stiff voltage source emulating the main grid while EPC_2 is disabled. The initial condition is the final of the previous test in subfigures (a)-(b) and with a balanced three-phase load connected. The disconnection does not bring to visible effects on the instantaneous voltages, proving the capability of providing the required load current and of forming the local grid voltage while operating islanded. By a more precise

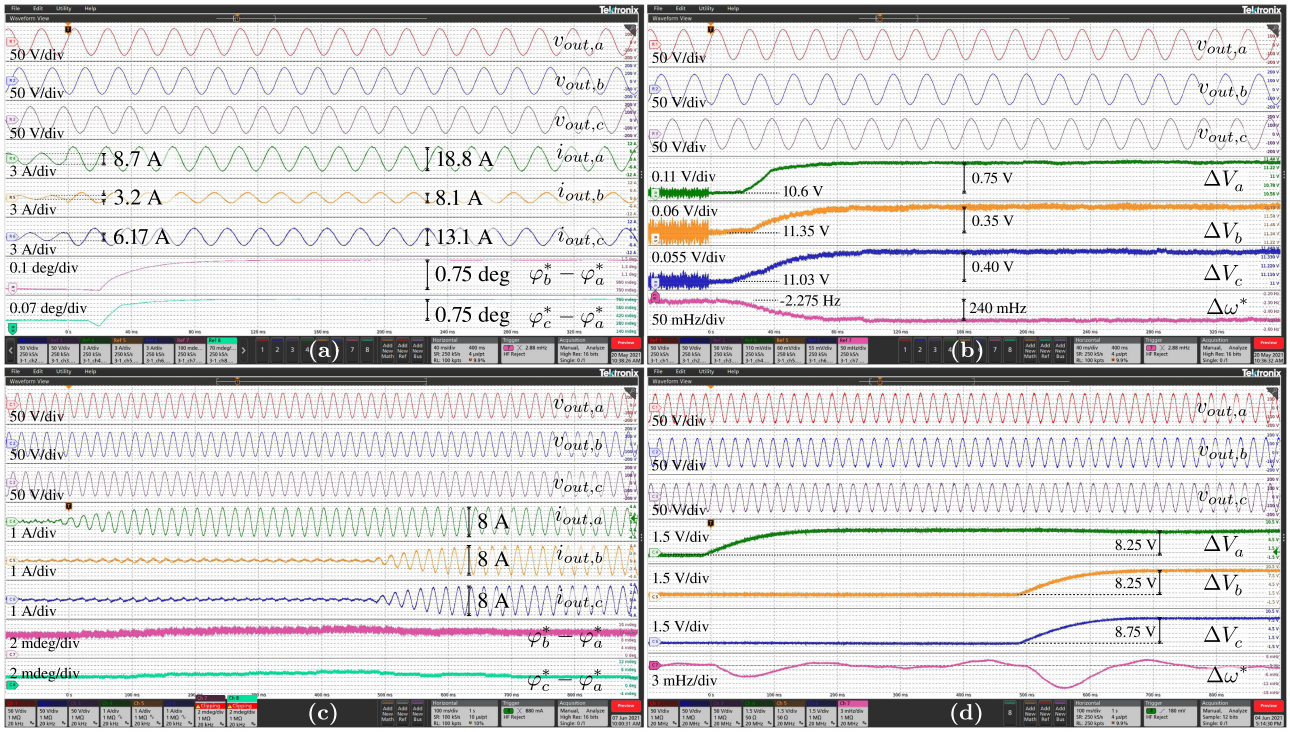

FIGURE 8. Experimental results with EPCs in Fig. 5 implementing the proposed control scheme in Fig. 3. (a)-(b) islanded operation with two EPCs and unbalanced load *a-N* : 16.7 Ω, *b-N* : 50.0 Ω, *c-N* : 25.0 Ω; (c)-(d) reference step change of EPC$_1$, Q_a^{ref} : 0 → 300 VAr and, subsequently, Q_b^{ref}, Q_c^{ref} : 0 → 300 VAr, with balanced load of 50 Ω.

inspection, Fig. 7(e) shows a transient phase-displacement, especially involving phase-*c*, which brings back to zero after the transient. Fig. 7(f) shows an increase of the voltage amplitude of all the phases due to the balanced reactive power absorption while islanded. The frequency ω^* decreases according to the chosen droop coefficient $k_{p,3\phi}$ and the total generated active power. Fig. 10 displays a zoomed-in view of the transition. Notably, perturbations of limited amplitude and lasting just a small fraction of the line period can be noticed across the instant of disconnection from the main grid.

The same transition is also shown in Fig. 7(g)-(h) with both the EPCs initially connected to the grid operating at non-nominal conditions, with grid frequency of about 50.22 Hz. A smooth transition can be observed also in this case.

D. PARALLEL OPERATION WHILE ISLANDED

Fig. 8(a)-(b) displays the parallel operation of EPC$_1$ and EPC$_2$ while disconnected from the main grid and the disconnection of EPC$_2$. The initial condition is the final one of the previous test in subfigures Fig. 7(e)-(f), but with an unbalanced load connected and the two EPCs active and equally sharing the load power. Then, EPC$_2$ is disconnected. This causes the operating frequency to transit from 47.73 Hz to 47.49 Hz, visibile in Fig. 8(b), indicating a load increase of about 850 W for EPC$_1$. Notably, the converters are able to keep synchronized and nicely share the load among them.

E. REACTIVE POWER CONTROL

Fig. 8(c)-(d) shows the reactive power control capability of the solution. Firstly, a step change is applied to phase-*a*, from 0 to 300 VAr, then, subsequently, the same step change is applied to phase-*b* and phase-*c* as well. The main effect is an increase of ΔV_x, according to the linearized models (8)-(9). Remarkably, reactive power is less critical than active power in terms of per-phase power control, because it consists in regulating the amplitude of the different phases, without significant effects on the other phases and the synchronization with the grid.

F. ISLANDED TO GRID-CONNECTED TRANSITION

The transition from the islanded to the grid-connected operation can be managed as commonly done in microgrids with distributed EPCs that implement the traditional droop control. Such kind of transition is briefly discussed in this subsection for completeness and demonstration purposes.

The synchronization of an islanded system to a grid voltage may be performed, for example, as discussed in [6], that is, by setting:

$$\omega_0 = \omega_g^{\text{nom}} + k_{i,\varphi}^{\text{synch}} \int \varphi_{MG} - \varphi_g \, \mathrm{d}t \tag{23}$$

$$V_0 = V_g^{\text{nom}} + k_{i,V}^{\text{synch}} \int V_{MG} - V_g \, \mathrm{d}t \tag{24}$$

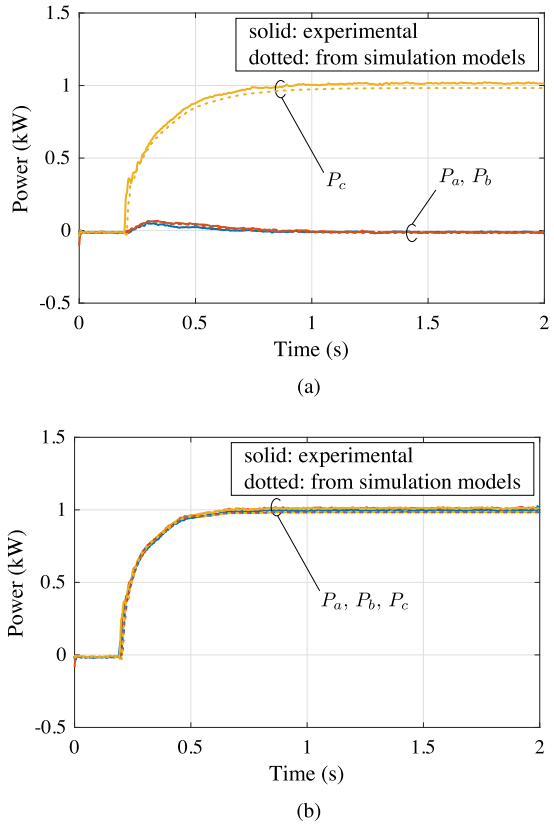

FIGURE 9. **Output power response to step reference changes considering experimental and simulation models. (a) step change of phase-*c* power reference; (b) step change of the power references of all the three phases.**

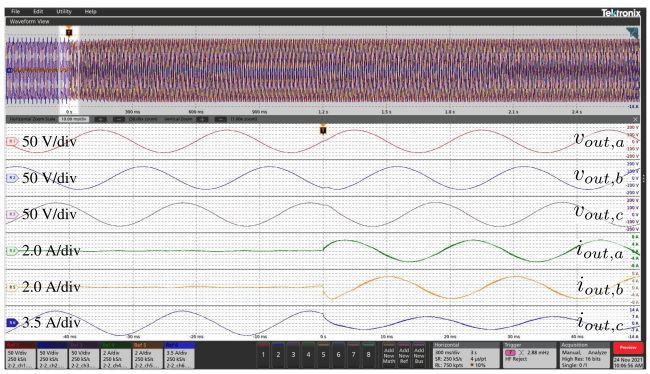

FIGURE 10. **Detail of the grid-connected to islanded transition in Fig. 7(e)-(f).**

where φ_g and V_g are the grid voltage phase angle and amplitude, respectively, while φ_{MG} and V_{MG} are the phase angle and amplitude of the islanded microgrid voltage, respectively. The phase angle $\varphi_{3\phi}$ and the mean voltage amplitude of the EPC that is closest to the circuit breaker *CB* constitute a good choice for φ_{MG} and V_{MG}, respectively. The integrative gains $k_{i,\varphi}^{\text{synch}}$, $k_{i,V}^{\text{synch}}$ should be set based on the desired speed of response (e.g., 1-10 s). PI regulators may be used as well to achieve faster dynamics.

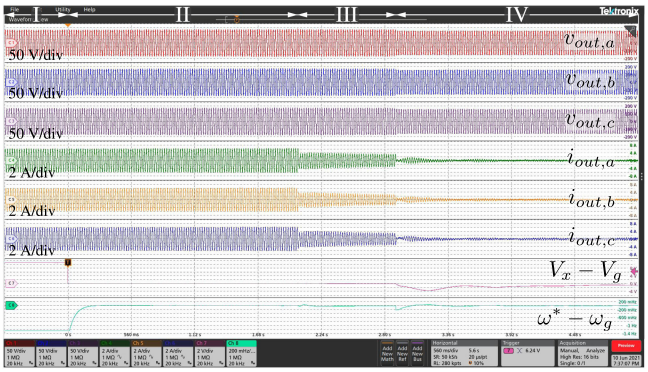

FIGURE 11. **Islanded into grid-connected transition of EPCs. Islanded operation is established in stage I, synchronization to the grid is performed in stage II, connection to the grid takes place at the beginning of stage III, per-phase control is activated for both the converters at the beginning of stage IV.**

The resulting transition is shown in Fig. 11, displaying the reconnection of the EPCs to the main grid. Four stages may be distinguished, marked at the top of the same figure: *i)* islanded operation, when the EPCs operate as droop-controlled converters as discussed in Section II-B, *ii)* synchronization to the grid voltage by means of (23)-(24), which reduces to zero the signals $V_x - V_g$, $\omega^* - \omega_g$, and the angle difference with the main grid, *iii)* connection to the grid by closing the circuit breaker *CB* in Fig. 2, *iv)* activation of the per-phase control. Remarkably, no overcurrents are present at the connection with the grid (i.e., across stage III and IV), demonstrating an accurate synchronization. At the beginning of stage IV the per-phase control is activated with zero power references for all the phases, demonstrating the possibility to restore the proposed per-phase power control smoothly during grid-tied operation.

V. CONCLUSION

In this paper, a per-phase power controller is presented for three-phase four-wires grid-tied inverters that is capable of *i*) independent output power tracking for each phase while operating grid-connected, *ii*) smooth transitions into the islanded operation, *iii*) operation in islanded conditions even when multiple parallel connected converters integrating the proposed controller are present. The controller extends the functionalities of voltage-controlled inverters using traditional droop laws, allowing grid-connected operation and the independent control of the output power at each phase of the inverter. By the proposed structure, the capability of droop-like approaches of seamlessly transit into the islanded operation is preserved. The challenge in jointly providing per-phase output power control during grid-tied operation and seamless islanded transitions stems from the fact that output active-power control is done by adjusting the frequency of the phase voltage, according to the traditional droop laws. In practice, these adjustments are necessarily different among the different inverter phases, bringing to phase voltages with different frequencies in case of absence of a stiff grid voltage. For

this reason the transition into islanded operation is particularly critical. The proposed solution is based on a three-phase synchronization loop, acting on all the three phases of the inverter, with parallel power regulators to achieve per-phase power control. In the paper, the controller is analyzed and a simple design procedure is devised. Experimental results are reported to show the operation of inverter prototypes driven by the proposed controller. The obtained results show that the controller fulfills the expected features with well damped dynamics, in accordance with the design. The controller can be employed in microgrids where output power tracking of distributed inverters is needed and smooth transitions into islanded operation due to unexpected events are possible. Finally, adaptation of the controller for three-phase inverters without the neutral connection is potentially possible and will be object of future studies.

REFERENCES

[1] *IEA (2020), World energy outlook 2020*, *IEA*, Paris, 2020. [Online]. Available: https://www.iea.org/reports/world-energy-outlook-2020

[2] A. Mohammed, S. S. Refaat, S. Bayhan, and H. Abu-Rub, "AC microgrid control and management strategies: Evaluation and review," *IEEE Power Electron. Mag.*, vol. 6, no. 2, pp. 18–31, Jun. 2019.

[3] S. Chandak and P. K. Rout, "Microgrids during the outbreak of COVID-19," *IEEE Smart Grid Newslett.*, Jul. 2020.

[4] M. Shahidehpour, M. Yan, P. Shikhar, S. Bahramirad, and A. Paaso, "Blockchain for peer-to-peer transactive energy trading in networked microgrids: Providing an effective and decentralized strategy," *IEEE Electrif. Mag.*, vol. 8, no. 4, pp. 80–90, Dec. 2020.

[5] A. S. Vijay, S. Doolla, and M. C. Chandorkar, "Unbalance mitigation strategies in microgrids," *IET Power Electron.*, vol. 13, no. 9, pp. 1687–1710, 2020.

[6] J. M. Guerrero, J. C. Vasquez, J. Matas, L. G. de Vicuna, and M. Castilla, "Hierarchical control of droop-controlled AC and DC microgrids-a general approach toward standardization," *IEEE Trans. Ind. Electron.*, vol. 58, no. 1, pp. 158–172, Jan. 2011.

[7] Y. Shi, W. Wu, H. Wang, Y. Du, and J. Su, "The parallel multi-inverter system based on the voltage-type droop control method," *IEEE Trans. Emerg. Sel. Topics Power Electron.*, vol. 4, no. 4, pp. 1332–1341, Dec. 2016.

[8] J. Rocabert, A. Luna, F. Blaabjerg, and P. Rodríguez, "Control of power converters in AC microgrids," *IEEE Trans. Power Electron.*, vol. 27, no. 11, pp. 4734–4749, Nov. 2012.

[9] R. H. Lasseter, Z. Chen, and D. Pattabiraman, "Grid-forming inverters: A critical asset for the power grid," *IEEE Trans. Emerg. Sel. Topics Power Electron.*, vol. 8, no. 2, pp. 925–935, Jun. 2020.

[10] Q. Liu, T. Caldognetto, and S. Buso, "Review and comparison of grid-tied inverter controllers in microgrids," *IEEE Trans. Power Electron.*, vol. 35, no. 7, pp. 7624–7639, Jul. 2020.

[11] A. Timbus, M. Liserre, R. Teodorescu, P. Rodriguez, and F. Blaabjerg, "Evaluation of current controllers for distributed power generation systems," *IEEE Trans. Power Electron.*, vol. 24, no. 3, pp. 654–664, Mar. 2009.

[12] R. Rosso, X. Wang, M. Liserre, X. Lu, and S. Engelken, "Grid-forming converters: Control approaches, grid-synchronization, and future trends-a review," *IEEE Open J. Ind. Appl.*, vol. 2, pp. 93–109, 2021, doi: 10.1109/OJIA.2021.3074028.

[13] R. Rosso, X. Wang, M. Liserre, X. Lu, and S. Engelken, "Grid-forming converters: An overview of control approaches and future trends," in *Proc. IEEE Energy Convers. Congr. Expo.*, 2020, pp. 4292–4299.

[14] H. Han, X. Hou, J. Yang, J. Wu, M. Su, and J. M. Guerrero, "Review of power sharing control strategies for islanding operation of AC microgrids," *IEEE Trans. Smart Grid*, vol. 7, no. 1, pp. 200–215, Jan. 2016.

[15] "IEEE Guide for Distributed Energy Resources Management Systems (DERMS) Functional Specification," in *IEEE Std 2030.11-2021*, pp. 1–65, Jun. 2021, doi: 10.1109/IEEESTD.2021.9447316.

[16] S. Lissandron and P. Mattavelli, "A controller for the smooth transition from grid-connected to autonomous operation mode," in *Proc. IEEE Energy Convers. Congr. Expo.*, 2014, pp. 4298–4305.

[17] J. M. Guerrero, L. Hang, and J. Uceda, "Control of distributed uninterruptible power supply systems," *IEEE Trans. Ind. Electron.*, vol. 55, no. 8, pp. 2845–2859, Aug. 2008.

[18] M. A. Abusara, J. M. Guerrero, and S. M. Sharkh, "Line-interactive UPS for microgrids," *IEEE Trans. Ind. Electron.*, vol. 61, no. 3, pp. 1292–1300, Mar. 2014.

[19] H. Abedini, T. Caldognetto, P. Mattavelli, and P. Tenti, "Real-time validation of power flow control method for enhanced operation of microgrids," *Energies*, vol. 13, no. 22, 2020, Art. no. 5959. [Online]. Available: https://www.mdpi.com/1996-1073/13/22/5959

[20] J. Wang, N. Zhou, Y. Ran, and Q. Wang, "Optimal operation of active distribution network involving the unbalance and harmonic compensation of converter," *IEEE Trans. Smart Grid*, vol. 10, no. 5, pp. 5360–5373, Sep. 2019.

[21] F. H. M. Rafi, M. Hossain, M. S. Rahman, and S. Taghizadeh, "An overview of unbalance compensation techniques using power electronic converters for active distribution systems with renewable generation," *Renewable Sustain. Energy Rev.*, vol. 125, 2020, Art. no. 109812.

[22] P. Tenti and T. Caldognetto, "On microgrid evolution to local area energy network (E-LAN)," *IEEE Trans. Smart Grid*, vol. 10, no. 2, pp. 1567–1576, Mar. 2019.

[23] D. I. Brandao, L. S. Araujo, A. M. S. Alonso, G. L. dos Reis, E. V. Liberado, and F. P. Marafão, "Coordinated control of distributed three- and single-phase inverters connected to three-phase three-wire microgrids," *IEEE Trans. Emerg. Sel. Topics Power Electron.*, vol. 8, no. 4, pp. 3861–3877, Dec. 2020.

[24] C. Burgos-Mellado, R. Cárdenas, D. Sáez, A. Costabeber, and M. Sumner, "A control algorithm based on the conservative power theory for cooperative sharing of imbalances in four-wire systems," *IEEE Trans. Power Electron.*, vol. 34, no. 6, pp. 5325–5339, Jun. 2019.

[25] T. Caldognetto and P. Tenti, "Microgrids operation based on master-slave cooperative control," *IEEE Trans. Emerg. Sel. Topics Power Electron.*, vol. 2, no. 4, pp. 1081–1088, Dec. 2014.

[26] A. Mortezaei, M. G. Simões, M. Savaghebi, J. M. Guerrero, and A. Al-Durra, "Cooperative control of multi-master-slave islanded microgrid with power quality enhancement based on conservative power theory," *IEEE Trans. Smart Grid*, vol. 9, no. 4, pp. 2964–2975, Jul. 2018.

[27] P. Baez-Gonzalez, E. Rodriguez-Diaz, J. C. Vasquez, and J. M. Guerrero, "Peer-to-peer energy market for community microgrids [*Technology Leaders*]," *IEEE Electrific. Mag.*, vol. 6, no. 4, pp. 102–107, Sec. 2018.

[28] E. Espina, M. Espinoza, and R. Cárdenas, "Active power angle droop control per phase for unbalanced 4-wire microgrids," in *Proc. IEEE Southern Power Electron. Conf.*, 2017, pp. 1–6.

[29] B. Liu, Z. Liu, J. Liu, R. An, H. Zheng, and Y. Shi, "An adaptive virtual impedance control scheme based on small-AC-signal injection for unbalanced and harmonic power sharing in islanded microgrids," *IEEE Trans. Power Electron.*, vol. 34, no. 12, pp. 12 333–12 355, Dec. 2019.

[30] S. M. Fazeli, H. W. Ping, N. B. A. Rahim, and B. T. Ooi, "Individual-phase control of 3-phase 4-wire voltage-source converter," *IET Power Electron.*, vol. 7, no. 9, pp. 2354–2364, 2014.

[31] H. Abedini, T. Caldognetto, and P. Mattavelli, "A per-phase power controller allowing smooth transitions to islanded operation," in *Proc. IEEE Energy Convers. Congr. Expo.*, 2021, pp. 1–7.

[32] Q. Zhong and D. Boroyevich, "Structural resemblance between droop controllers and phase-locked loops," *IEEE Access*, vol. 4, pp. 5733–5741, 2016.

[33] M. B. Delghavi and A. Yazdani, "A unified control strategy for electronically interfaced distributed energy resources," *IEEE Trans. Power Del.*, vol. 27, no. 2, pp. 803–812, Apr. 2012.

[34] Y. A. I. Mohamed and E. F. El-Saadany, "Adaptive decentralized droop controller to preserve power sharing stability of paralleled inverters in distributed generation microgrids," *IEEE Trans. Power Electron.*, vol. 23, no. 6, pp. 2806–2816, Nov. 2008.

[35] G. Yajuan, W. Weiyang, G. Xiaoqiang, and G. Herong, "An improved droop controller for grid-connected voltage source inverter in microgrid," in *Proc. 2nd Int. Symp. Power Electron. Distrib. Gener. Syst.*, 2010, pp. 823–828.

[36] W. Yao, M. Chen, J. Matas, J. M. Guerrero, and Z. Qian, "Design and analysis of the droop control method for parallel inverters considering

the impact of the complex impedance on the power sharing," *IEEE Trans. Ind. Electron.*, vol. 58, no. 2, pp. 576–588, Feb. 2011.
[37] D. Pan, X. Wang, F. Liu, and R. Shi, "Transient stability of voltage-source converters with grid-forming control: A design-oriented study," *IEEE Trans. Emerg. Sel. Topics Power Electron.*, vol. 8, no. 2, pp. 1019–1033, Jun. 2020.
[38] K. De Brabandere, B. Bolsens, J. Van den Keybus, A. Woyte, J. Driesen, and R. Belmans, "A voltage and frequency droop control method for parallel inverters," *IEEE Trans. Power Electron.*, vol. 22, no. 4, pp. 1107–1115, Jul. 2007.
[39] Q.-C. Zhong, J. Liang, G. Weiss, C. Feng, and T. Green, "H^{∞}control of the neutral point in four-wire three-phase DC-AC converters," *IEEE Trans. Ind. Electron.*, vol. 53, no. 5, pp. 1594–1602, Oct. 2006.
[40] J. Liang, T. C. Green, C. Feng, and G. Weiss, "Increasing voltage utilization in split-link, four-wire inverters," *IEEE Trans. Power Electron.*, vol. 24, no. 6, pp. 1562–1569, Jun. 2009.
[41] L. Vandevelde, "DC-bus voltage balancing controllers for split DC-link four-wire inverters and their impact on the quality of the injected currents," *CIRED - Open Access Proc. J.*, vol. 2017, no. 4, pp. 564–568, Oct. 2017.

TOMMASO CALDOGNETTO (Senior Member, IEEE) received the M.S. (Hons.) degree in electronic engineering and the Ph.D. degree in information engineering from the University of Padova, Padova, Italy, in 2012 and 2016, respectively. He is currently an Assistant Professor with the Department of Management and Engineering, University of Padova, Vicenza, Italy. His research interests include the control of grid-tied converters, microgrid architectures, converters for dc nanogrids, and real-time simulation for power electronics applications.

HOSSEIN ABEDINI (Student Member, IEEE) received the M.S. (Hons.) and B.Sc. degrees in telecommunication engineering and the M.Sc. degree in power electronics engineering from the University of Shahid Beheshti, Tehran, Iran, in 2013 and 2016, respectively. He is currently working toward the Ph.D. degree in power electronics with the University of Padova, Padua, Italy. His research interests include smart DC/AC microgrids, digital control, power converters, and inverters.

PAOLO MATTAVELLI (Fellow, IEEE) received the M.S. (Hons.) and Ph.D. degrees in electrical engineering from the University of Padova, Padova, Italy, in 1992 and 1995, respectively. From 1995 to 2001, he was a Researcher with the University of Padova. From 2001 to 2005, he was an Associate Professor with the University of Udine, Udine, Italy, where he led Power Electronics Laboratory. In 2005, he joined the University of Padova, with the same duties. From 2010 to 2012, he was with the Center for Power Electronics Systems, Virginia Tech, Blacksburg, VA, USA. He is currently a Professor with the University of Padova. In his research fields, he has been leading several industrial and government projects. His current Google scholar H-index is 80. His major research interests include analysis, modeling, and analog and digital control of power converters, grid-connected converters for renewable energy systems and microgrids, and high-temperature and high-power-density power electronics. From 2003 to 2012, he was an Associate Editor for the IEEE TRANSACTIONS ON POWER ELECTRONICS. He is the Co-Editor-in-Chief of the IEEE TRANSACTIONS ON POWER ELECTRONICS. From 2005 to 2010, he was the Industrial Power Converter Committee Technical Review Chair for the IEEE TRANSACTIONS ON INDUSTRY APPLICATIONS. From 2003 to 2006, 2006 to 2009, and 2013 to 2015, he was a Member-at-Large of the IEEE Power Electronics Society's Administrative Committee. He was the recipient of the Prize Paper Award in the IEEE TRANSACTIONS ON POWER ELECTRONICS in 2005, 2006, 2011, and 2012, and the 2nd Prize Paper Award at the IEEE Industry Applications Society Annual Meeting in 2007.